

# Geology of the Northern Norrbotten ore province, northern Sweden

Paper 10 (13)

Editor: Stefan Bergman



**SGU**

Sveriges geologiska undersökning  
Geological Survey of Sweden



Rapporter och meddelanden 141

# **Geology of the Northern Norrbotten ore province, northern Sweden**

Editor: Stefan Bergman

Sveriges geologiska undersökning  
2018

ISSN 0349-2176  
ISBN 978-91-7403-393-9

**Cover photos:**

*Upper left:* View of Torneälven, looking north from Sakkaravaara, northeast of Kiruna. *Photographer:* Stefan Bergman.

*Upper right:* View (looking north-northwest) of the open pit at the Aitik Cu-Au-Ag mine, close to Gällivare. The Nautanen area is seen in the background. *Photographer:* Edward Lynch.

*Lower left:* Iron oxide-apatite mineralisation occurring close to the Malmberget Fe-mine. *Photographer:* Edward Lynch.

*Lower right:* View towards the town of Kiruna and Mt. Luossavaara, standing on the footwall of the Kiruna apatite iron ore on Mt. Kiirunavaara, looking north. *Photographer:* Stefan Bergman.

*Head of department, Mineral Resources:* Kaj Lax

*Editor:* Stefan Bergman

*Layout:* Tone Gellerstedt och Johan Sporrang, SGU

*Print:* Elanders Sverige AB

Geological Survey of Sweden  
Box 670, 751 28 Uppsala  
phone: 018-17 90 00  
fax: 018-17 92 10  
e-mail: sgu@sgu.se  
www.sgu.se

# Table of Contents

<b>Introduktion (in Swedish)</b> .....	<b>6</b>
<b>Introduction</b> .....	<b>7</b>
<b>1. Regional geology of northern Norrbotten County</b> .....	<b>9</b>
References .....	14
<b>2. Geology, lithostratigraphy and petrogenesis of c. 2.14 Ga greenstones in the Nunasvaara and Masugnsbyn areas, northernmost Sweden</b> .....	<b>19</b>
Abstract .....	19
Introduction .....	20
Regional setting of Norrbotten greenstone belts .....	21
Geology of the Nunasvaara and Masugnsbyn greenstone successions .....	23
Petrogenesis of the greenstones: Preliminary U-Pb geochronology, litho-geochemistry and Sm-Nd isotopic results .....	52
Summary and conclusions .....	68
Acknowledgements .....	69
References .....	70
<b>3. Stratigraphy and ages of Palaeoproterozoic metavolcanic and metasedimentary rocks at Käymäjärvi, northern Sweden</b> .....	<b>79</b>
Abstract .....	79
Introduction .....	80
General geology .....	80
Structure and stratigraphy of the Käymäjärvi area .....	81
Sample description .....	89
Analytical methods .....	90
Analytical results .....	91
Discussion .....	96
Conclusions .....	100
Acknowledgements .....	101
References .....	101
<b>4. Petrological and structural character of c. 1.88 Ga meta-volcanosedimentary rocks hosting iron oxide-copper-gold and related mineralisation in the Nautanen–Aitik area, northern Sweden</b> .....	<b>107</b>
Abstract .....	107
Introduction .....	108
Regional setting .....	108
Geology of the Nautanen–Aitik area .....	110
Structural geology and deformation .....	132
Summary and Conclusions .....	144
Acknowledgements .....	144
References .....	145
<b>5. Age and lithostratigraphy of Svecofennian volcanosedimentary rocks at Masugnsbyn, northernmost Sweden – host rocks to Zn-Pb-Cu- and Cu ±Au sulphide mineralisations</b> .....	<b>151</b>
Abstract .....	151
Introduction .....	152
Geological overview .....	153
Discussion and preliminary conclusions .....	194
Acknowledgements .....	197
References .....	198

<b>6. Folding observed in Palaeoproterozoic supracrustal rocks in northern Sweden</b>	<b>205</b>
Abstract	205
Introduction	205
Geological setting	207
Structural geological models	209
Geophysical data	212
Discussion and Conclusions	251
References	255
<b>7. The Pajala deformation belt in northeast Sweden:</b>	
<b>Structural geological mapping and 3D modelling around Pajala</b>	<b>259</b>
Abstract	259
Geological setting	259
Structural analysis	263
2D regional geophysical modelling and geological interpretation	272
Local and semi-regional 3D models	274
Discussion	280
Conclusions	283
References	284
<b>8. The Vakko and Kovo greenstone belts north of Kiruna:</b>	
<b>Integrating structural geological mapping and geophysical modelling</b>	<b>287</b>
Abstract	287
Introduction	287
Geological setting	289
Geophysical surveys	291
Results	296
Discussion	306
Conclusions	308
References	309
<b>9. Geophysical 2D and 3D modelling in the areas around</b>	
<b>Nunasvaara and Masugnsbyn, northern Sweden</b>	<b>311</b>
Abstract	311
Nunasvaara	312
2D modelling of profile 1 and 2	316
Masugnsbyn	321
Regional modelling	329
Conclusion	338
References	339
<b>10. Imaging deeper crustal structures by 2D and 3D modelling of geophysical data.</b>	
<b>Examples from northern Norrbotten</b>	<b>341</b>
Abstract	341
Introduction	341
Methodology	342
Geological setting	342
Results	345
Conclusion	358
Outlook	358
Acknowledgements	358
References	359

<b>11. Early Svecokarelian migmatisation west of the Pajala deformation belt, northeastern Norrbotten province, northern Sweden</b>	<b>361</b>
Abstract	361
Introduction	362
Geology of the Masugnsbyn area	362
Discussion	372
Conclusions	374
Acknowledgements	375
References	376
<b>12. Age and character of late-Svecokarelian monzonitic intrusions in northeastern Norrbotten, northern Sweden</b>	<b>381</b>
Abstract	381
Introduction	381
Geological setting	382
Analytical methods	387
Analytical results	388
Discussion	393
Conclusions	396
Acknowledgements	396
References	397
<b>13. Till geochemistry in northern Norrbotten –regional trends and local signature in the key areas</b>	<b>401</b>
Abstract	401
Introduction	401
Glacial geomorphology and quaternary stratigraphy of Norrbotten	403
Samples and methods	406
Results and discussion	407
Conclusions	426
Acknowledgements	427
References	427

# Introduktion

Stefan Bergman & Ildikó Antal Lundin

Den här rapporten presenterar de samlade resultaten från ett delprojekt inom det omfattande tvärvetenskapliga Barentsprojektet i norra Sverige. Projektet initierades av Sveriges geologiska undersökning (SGU) som ett första led i den svenska mineralstrategin. SGU fick ytterligare medel av Näringsdepartementet för att under en fyraårsperiod (2012–2015) samla in nya geologiska, geofysiska och geokemiska data samt för att förbättra de geologiska kunskaperna om Sveriges nordligaste län. Det statligt ägda gruvbolaget LKAB bidrog också till finansieringen. Projektets strategiska mål var att, genom att tillhandahålla uppdaterad och utförlig geovetenskaplig information, stödja prospekterings- och gruvindustrin för att förbättra Sveriges konkurrenskraft inom mineralnäringen. Ny och allmänt tillgänglig geovetenskaplig information från den aktuella regionen kan hjälpa prospekterings- och gruvföretag att minska sina risker och prospekteringskostnader och främjar därigenom ekonomisk utveckling. Dessutom bidrar utökad geologisk kunskap till en effektiv, miljövänlig och långsiktigt hållbar resursanvändning. All data som har samlats in i projektet lagras i SGUs databaser och är tillgängliga via SGU.

Syftet med det här delprojektet var att få en djupare förståelse för den stratigrafiska uppbyggnaden och utvecklingen av de mineraliserade ytbergarterna i nordligaste Sverige. Resultaten, som är en kombination av ny geologisk kunskap och stora mängder nya data, kommer att gynna prospekterings- och gruvindustrin i regionen i många år framöver.

Norra Norrbottens malmprovins står för en stor del av Sveriges järn- och kopparmalmsproduktion. Här finns fyra aktiva metallgruvor (mars 2018) och mer än 500 dokumenterade mineraliseringar. Fyndigheterna är av många olika slag, där de viktigaste typerna är stratiforma kopparmineraliseringar, järnformationer, apatitjärnmalm av Kirunatyp och epigenetiska koppar-guldmineraliseringar. En vanlig egenskap hos de flesta malmer och mineraliseringar i Norr- och Västerbotten är att de har paleoproterozoiska vulkaniska och sedimentära bergarter som värdbergart. För undersökningarna valdes ett antal nyckelområden med bästa tillgängliga blottningsgrad. De utvalda områdena representerar tillsammans en nästan komplett stratigrafi i ytbergarter inom åldersintervallet 2,5–1,8 miljarder år.

Rapporten består av tretton kapitel och inleds med en översikt över de geologiska förhållandena, som beskriver huvuddragen i de senaste resultaten. Översikten följs av fyra kapitel (2–5) som huvudsakligen handlar om litostratigrafi och åldersbestämningar av ytbergarterna. Huvudämnet för de därpå följande fem kapitlen (6–10) är 3D-geometri och strukturell utveckling. Därefter kommer två kapitel (11–12) som fokuserar på U-Pb-datering av en metamorf respektive intrusiv händelse. Rapporten avslutas med en studie av geokemin hos morän i Norra Norrbottens malmprovins (kapitel 13).

# Introduction

Stefan Bergman & Ildikó Antal Lundin

This volume reports the results from a subproject within the Barents Project, a major programme in northern Sweden. The multidisciplinary Barents Project was initiated by SGU as the first step in implementing the Swedish National Mineral Strategy. SGU obtained additional funding from the Ministry of Enterprise and Innovation to gather new geological, geophysical and till geochemistry data, and generally enhance geological knowledge of northern Sweden over a four-year period (2012–2015). The state-owned iron mining company LKAB also helped to fund the project. The strategic goal of the project was to support the exploration and mining industry, so as to improve Sweden's competitiveness in the mineral industry by providing modern geoscientific information. Geological knowledge facilitates sustainable, efficient and environmentally friendly use of resources. New publicly available geoscientific information from this region will help exploration and mining companies to reduce their risks and exploration costs, thus promoting economic development. All data collected within the project are stored in databases and are available at SGU.

This subproject within the Barents Project aims to provide a deeper understanding of the stratigraphy and depositional evolution of mineralised supracrustal sequences in northernmost Sweden. The combined results in the form of new geological knowledge and plentiful new data will benefit the exploration and mining industry in the region for many years to come.

The Northern Norrbotten ore province is a major supplier of iron and copper ore in Sweden. There are four active metal mines (March 2018) and more than 500 documented mineralisations. A wide range of deposits occur, the most important types being stratiform copper deposits, iron formations, Kiruna-type apatite iron ores and epigenetic copper-gold deposits. A common feature of most deposits is that they are hosted by Palaeoproterozoic metavolcanic or metasedimentary rocks. A number of key areas were selected across parts of the supracrustal sequences with the best available exposure. The areas selected combine to represent an almost complete stratigraphic sequence.

This volume starts with a brief overview of the geological setting, outlining some of the main recent achievements. This is followed by four papers (2–5) dealing mainly with lithostratigraphy and age constraints on the supracrustal sequences. 3D geometry and structural evolution are the main topics of the next set of five papers (6–10). The following two contributions (11–12) focus on U-Pb dating of a metamorphic event and an intrusive event, respectively. The volume concludes with a study of the geochemical signature of till in the Northern Norrbotten ore province (13).

**Authors, paper 10:**

*Mehrdad Bastani*

Geological Survey of Sweden  
Department of Mineral Resources,  
Uppsala, Sweden

*Ildiko Antal Lundin*

Geological Survey of Sweden  
Department of Mineral Resources,  
Uppsala, Sweden

*Shunguo Wang*

Uppsala University,  
Department of Earth Sciences,  
Uppsala, Sweden

*Stefan Bergman*

Geological Survey of Sweden  
Department of Mineral Resources,  
Uppsala, Sweden

# 10. Imaging deeper crustal structures by 2D and 3D modelling of geophysical data. Examples from northern Norrbotten

Mehrdad Bastani, Ildiko Antal Lundin, Shunguo Wang & Stefan Bergman

## ABSTRACT

Geophysical measurements were carried out by SGU in an area between Kiruna and Vittangi in northern Norrbotten, Sweden. The purpose of this study is to improve knowledge of the geology using modern methods, thereby creating supporting material for the exploration and mining industry in the region. In the summer of 2012 a 74 km long reflection seismic profile was acquired between Kiruna and Vittangi with the objective of imaging bedrock contacts and the geometry of structures at depth. In 2014 the seismic profile was followed up with magnetotelluric (MT) measurements aimed at modelling the variation in electrical resistivity of the upper crustal structures. In this study we present models from the 3D inversions of MT, magnetic and gravity field data. We compare the results with those from the reflection seismic data to reveal some of the details of the physical properties, the geometry of upper crustal structures and the bedrock in the study area. The analysis of the models to a depth of 5 km along five selected sections demonstrates a reasonable correlation between the modelled physical properties, although some differences are observed. The reflection seismic and susceptibility models have better resolution in imaging shallower structures such as folds and smaller-scale structures, due to denser data sampling and higher sensitivity. However, the deeper structures (>2 km) seen in the reflection seismic image correlate better with the density and resistivity models. Towards the eastern part of the area very low-electrical resistivity structures seen in the resistivity model coincide with a zone dominated by sulphide and graphite mineralisation. We propose a more detailed ground and airborne survey to identify potential areas for exploration.

## INTRODUCTION

Over the past few decades 2D and 3D modelling of geophysical data, such as gravity, magnetic, reflection seismic and electromagnetic data, has played a key role in imaging crustal structures as deep as tens of kilometres (England & Ebbing 2012, Arora et al. 2012, Hedin et al. 2014, Cherevatova et al. 2015, Kamm et al. 2015). The geophysical models are generated by either forward or inverse techniques. Forward modelling uses *a priori* knowledge of the physical properties of the bedrock in the study area,

for example, in the case of gravity field, density. The *a priori* knowledge is usually gained from laboratory measurements on the physical properties of rock samples or, in some cases, known values extracted from other surveys with similar geological settings. Forward modelling is therefore parameter driven: it assumes a property and finds the geometry of structures to fit the measured data. In inverse modelling, measured data determine the geometry and physical properties of the geological structures. There are two main inversion techniques: Finite Difference (FD) and Finite Element (FE). In FD modelling, the space is divided into cells of known geometry and the physical properties of each cell are estimated using an iterative mathematical method (Aster et al. 2005). In the FE method, the cells have irregular forms and both the geometry and physical properties are modelled. In this report we present the results from 3D modelling of gravity, magnetic and electromagnetic data collected by SGU in the vicinity of the town of Kiruna in northern Norrbotten County in Sweden. The main aim of this study is to produce a more detailed understanding of the depth extent of known geological units and structures. The reflection seismic data collected by SGU along a 74 km long profile (Juhojuntti et al. 2014) is used to check the validity of the models.

## METHODOLOGY

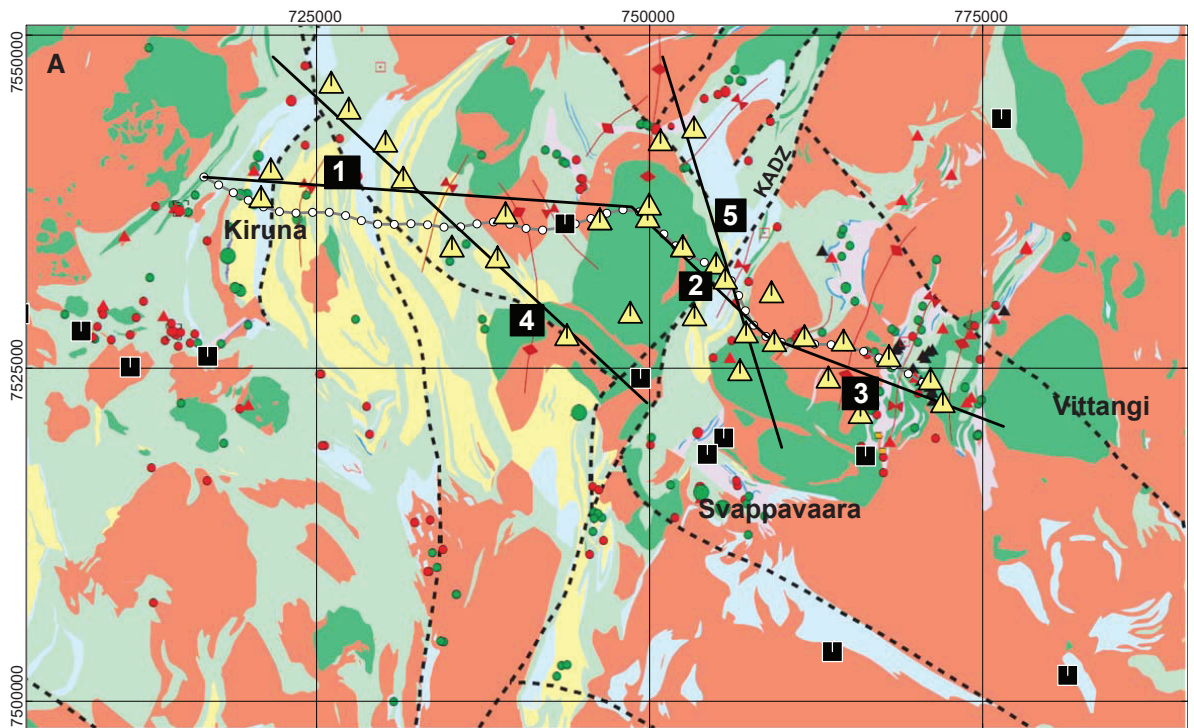
Existing data in SGU databases were compiled and mapped using GIS tools. These include ground gravity, airborne and ground magnetics, electromagnetic (VLF), natural gamma radiation, petrophysical and ground geological observation data. The data in the study area were then extracted and imported into geophysical software for further analyses. At several locations ground geophysical measurements were carried out to fill in gaps in the existing data. New geophysical data, such as reflection seismic and magnetotelluric (MT) data with reasonably great penetration depth (> 5 km), were also obtained. The geophysical data were then processed and modelled in 2D and 3D using an FD approach.

## GEOLOGICAL SETTING

The bedrock (Fig. 1A) represents part of the Svecokarlian orogen, formed 1.9–1.8 Ga ago, and includes Archaean and early Palaeoproterozoic rocks. The Råstojaure complex, north of Kiruna, consists of metagranitoids and subordinate metasupracrustal rocks formed, deformed and metamorphosed in the Archaean. These rocks are unconformably overlain by metaconglomerate, quartzite and metaandesitemetabasalt of the 12 km thick Kovo group (Martinsson 1999). The overlying Kiruna greenstone group (Martinsson 1997) is 14 km thick, consisting mainly of metabasalt with lesser amounts of metaultramafic rocks, graphite schist, iron formation and marble. This unit hosts the Viscaria copper deposit as well as a number of iron mineralisations. Mafic dyke swarms cut the Råstojaure complex, and mafic sills are common in the Kovo and Kiruna greenstone groups. The Svecofennian supracrustal rocks and several suites of intrusive rocks were formed during the Svecofennian orogeny. The Svecofennian supracrustal rocks unconformably overlie the Kiruna greenstone group, and consist of acidic, intermediate and basic metavolcanic, and clastic metasedimentary rocks with a total thickness greater than 3 km. Kiirunavaara iron ore and several other iron deposits occur within these metavolcanic rocks.

The youngest Svecofennian supracrustal rock in the area is a quartz-rich metasandstone (Hauki quartzite). Except for the youngest intrusive suite (Lina granite), all rocks in the area were affected by ductile deformation, hydrothermal alteration and greenschist to amphibolite facies metamorphism during the Svecofennian orogeny.

Nd isotopic studies have shown that Archaean rock is probably present in the subsurface north of a line between Luleå and Jokkmokk (Öhlander et al. 1993). It is therefore highly probable that Archaean rocks can be found at depth in the Kiruna area. The outcrop pattern suggests that the general dip of the units is to the south (Juhojuntti et al. 2014). During ductile deformation large folds with wavelengths of up to several kilometres were formed, with steep axial planes and south-plunging fold



- |  |   |   |
|--|---|---|
| ● Iron mine, in operation                        | ● Precious metal, trial pit or prospect     | ■ Iron mineralisation                                 |
| ● Iron mine, abandoned                           | ● Precious metal mineralization             | ■ Metadacite-rhyolite                                 |
| ● Iron ore, trial pit or prospect                | ▲ Quarry, industrial mineral, abandoned     | ■ Metabasalt-andesite                                 |
| ● Sulphide mine, abandoned                       | ▲ Industrial mineral, trial pit or prospect | ■ Carbonate rock                                      |
| ● Sulphide mineralization, trial pit or prospect | — Anticline and syncline                    | ■ Clastic metasedimentary rock                        |
| ● Sulphide mineralization                        | — — Shear zone                              | ■ Metasedimentary rock (phyllite to shists)           |
| □ Sulphide ore known from core drilling          |   | ■ Felsic intrusive rock, partly metamorphic           |
| ■ Other metal oxide mineralization               |   | ■ Mafic-ultramafic intrusive rock, partly metamorphic |

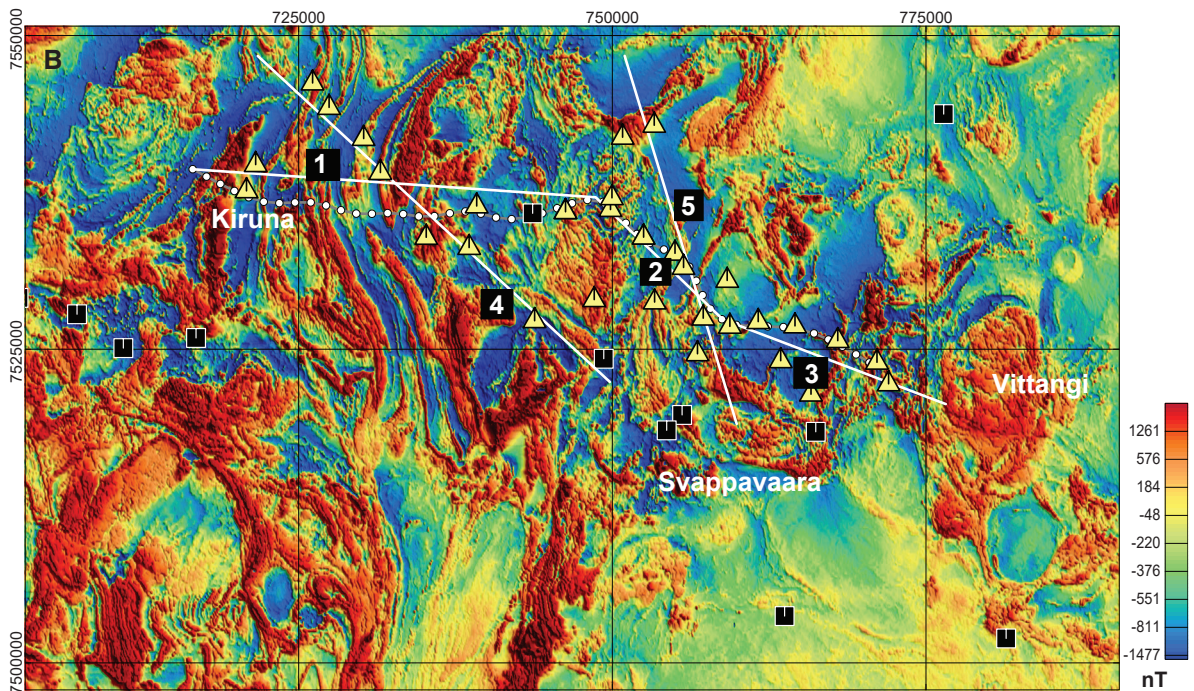


Figure 1. **A.** Simplified regional bedrock map of the study area (after Bergman et al. 2000). **B.** Map of total magnetic field anomaly.

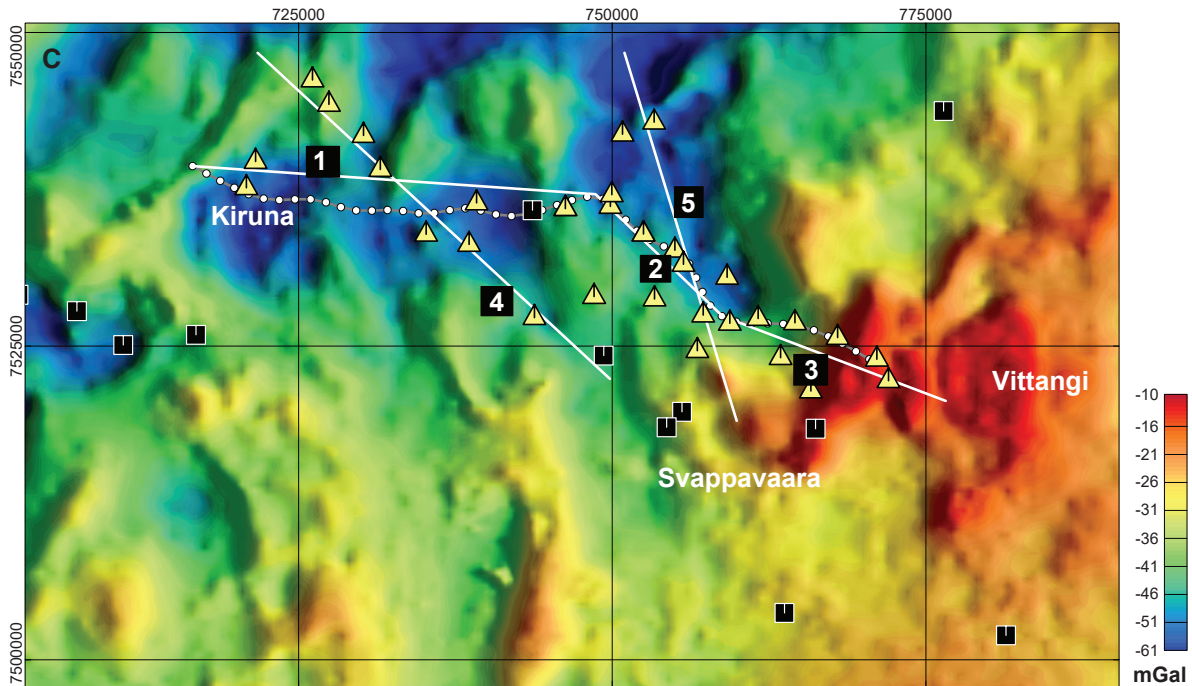


Figure 1. **C.** Bouguer anomaly map from ground measurements. The legends to the right in A show the bedrock and mineralisations in the area. The reflection seismic line is shown as a white line with white circles. The yellow triangles and the black squares are MT stations measured by SGU and Oulu University, respectively (see Bastani et al. 2015). The white lines with black squares (numbered in white) are the selected directions to show model sections from the 3D models (see Fig. 2D).

axes. In the eastern part of the area the structure is more complicated, with several folding phases in different orientations. Foliations developed with strongly variable intensity. Ductile shear zones separate more weakly deformed domains. The two most important shear zones are the Karesuando–Arjeplog deformation zone in the east and the Kiruna–Naimakka deformation zone in the west (Bergman et al. 2001), with widths of 810 km, including less deformed lenses. Ductile shear zones are commonly reactivated in the brittle regime. Some copper and gold mineralisations can be found along the Karesuando–Arjeplog deformation zone.

At the eastern end of the seismic profile (Fig. 1A) the Vittangi greenstone group (VGG), which forms the central part of the Nunasvaara key area, contains 61 mineral deposits, prospects or showings (Lynch & Jönberger 2013), the main commodity being graphite-bearing schists (e.g. Nunasvaara).

### Geophysical data

Airborne geophysical measurements were carried out by SGU during 1960–1964. The magnetic field was measured as a part of the iron inventory programme. Loussavaara–Kiirunavaara AB (LKAB) collected airborne data during 1979–1984. LKAB carried out airborne magnetic field, electromagnetic (both VLF and Slingram) and gamma ray radiation data acquisition. The survey direction was east–west. All airborne surveys in the area were made with a line separation of 200 m, a point distance of 40 m and a ground clearance of 30 m. The magnetic anomaly map (Fig. 1B) of the same area shown in Fig. 1A) reveals complicated patterns, such as banded, folded and circular features caused by supra-crustal and intrusive rocks. Those data contain valuable information about the deformation history of the rocks.

Regional gravity measurements were made by SGU and LMV during different periods, most intensively between 1960 and 1985. The distance between the measurement points varies between 300 and

3 000 metres. Gravity data (Fig. 1C) are usually shown in the form of Bouguer anomaly maps. The gravity highs can usually be related to mafic magmatic rocks at depth. Gravity lows coincide with the distribution of supracrustal rocks with felsic compositions. In summer 2012 a reflection seismic profile approximately 74 km long was acquired by SGU in the Kiruna area (shown by white circles in Figs. 1A–C). The main aim of the seismic measurements was to better understand the upper crustal structure in the Kiruna area, e.g. by imaging bedrock contacts and deformation zones. The western end of the seismic profile is only a few kilometres from the Kirunavaara mine, and close to the profile are several known mineralisation zones, some of which are active exploration targets. For more details of the data acquisition parameters the reader is referred to the report by Juhojuntti et al. (2014).

Magnetotelluric (MT) measurements were conducted in two areas (A and B) in northern Norrbotten during the summer of 2014 (Figs. 1A–C). The survey objectives were to model the variation of electrical resistivity of the upper crustal structures along the reflection seismic profile collected in the summer of 2012 (Juhojuntti et al. 2014) and to study the depth extent of known mineralisations. The collected MT signals cover a wide frequency band, from  $10^{-2}$  to 300 Hz. 2D and 3D modelling of the collected data images the variation of electrical resistivity down to depths > 30 km. Bastani et al. (2015) give a detailed account of the results from 2D modelling of collected MT data along two selected directions in two areas. Here we show the results from the 3D modelling of MT data in area A and, where necessary, compare them with the 2D modelling results.

## RESULTS

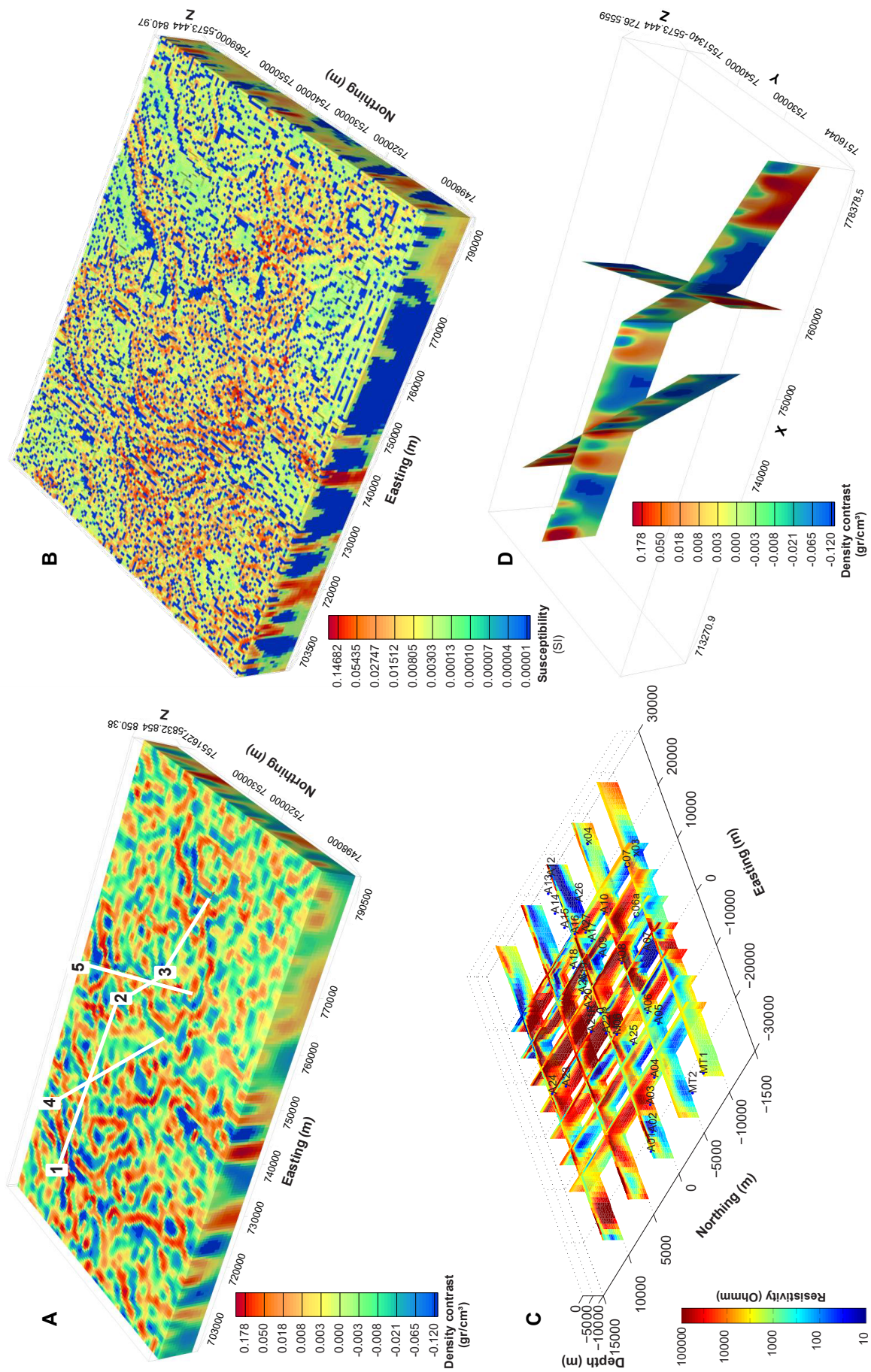
The VOXI program, a 3D finite difference inversion module supplied by Geosoft Company in the Oasis montaj software package was used for the 3D inversion of the potential field data. We tested several inversions using different parameter settings to obtain models as close as possible to the field and laboratory observations and measurements. The models resulting from 3D inversions of the gravity and magnetic field data are shown as density contrast and magnetic susceptibility in Figures 2A and 2B, respectively. The 3D inversion of the magnetic field and gravity data were made using model cells of 500 m × 500 m × 250 m in x, y and z directions, respectively. We used petrophysical data and constrained model susceptibility within the range of 0.00001 to 2.0 SI units. The unusually high-upper susceptibility limit of 2 was imposed to enable the inversion to take into account the several known iron ores in the area, of which the world-class Kiruna iron ore is best known. A density contrast of between –0.12 and 0.9 was used to constrain the density model.

We used the inversion code WSINV3DMT by Siripunvaraporn et al. (2005) to carry out 3D modelling of the data using a smoothing regularisation. The resulting 3D resistivity model is shown in Figure 2C. Note that the model is presented in the inversion's local coordinate system.

The MT data do not have sufficient resolution at the surface due to the low-frequency content of the signal. The susceptibility model shows higher frequency variations, which are mainly due to denser sampling and partly to the higher sensitivity of the method compared with gravity and MT.

### Selected susceptibility, resistivity and density sections from 3D models

Five portions of models numbered 1–5 that cross a few known geological structures and mineralised zones are selected to present more detailed results in the form of depth sections. The selected portions are shown on the density model in Figure 2A. The density contrast depth sections (here called sections) from the 3D models are shown in Figures 2A–2C. Sections 1 to 3 are collocated with three portions of the reflection seismic profile (Fig. 1) reported by Juhojuntti et al. (2014). The density contrast sections are shown in Figure 2D as an example. Along each direction we present model sections showing susceptibility, resistivity and density contrast. In each resistivity section we superimposed the contours of estimated susceptibilities and, on the upper part of the section, the bedrock geology. The location and type of known mineralisations are shown to facilitate comparison and interpretation.



◀ Figure 2. **A.** 3D density contrast model from the inversion of Bouguer anomaly data in the area. The selected section lines are shown in white. **B.** The 3D susceptibility model from the inversion of magnetic field anomaly data shown in Figure 1 B. **C.** Resistivity model from the 3D inversion of MT data. **D.** Density contrast sections taken from the model shown in a) along the selected sections (see Figure 1).

Comparison of the 3D models with the information in the reflection seismic data was rather difficult, mainly because of the weak reflection patterns seen in the seismic data. In a separate section we compare the seismic images with the 3D models, where a clear reflection pattern could be extracted to interpret regional structures in a more integrated manner.

### Section 1

This section is 32 km long and runs approximately west–east. Although distribution of the MT stations is sparse along section 1 (see Fig. 1) the 3D inversion model reveals valuable information along this section (Fig. 3). To make the comparison easier the modelled physical properties of various geological structures and units are summarised in Table 1.

The susceptibility model shows more details and resolves structures resembling major folds with varying dips that contain minor/smaller folds (higher frequency near surface susceptibility variations). The white and black arrows indicate the apparent average dips of major high- and low-magnetic susceptibility structures, respectively. The arrows are also shown on the resistivity and density contrast sections. For example, a few zones with susceptibilities  $>0.05$  ( $5000 \times 10^{-5}$  SI units) dip almost vertically in the mid-western part of the section. An easterly-dipping structure in the western part of the model and a steeply east-dipping structure in the middle of the model (close to 730000E) demonstrate variations in the dips of the modelled susceptibilities/structures, indicating folding structures present in the study area. The western to central part of the resistivity model is dominated by a low-resistivity zone with very faint high-resistivity structures. However, the lowest resistivity zones correlate very well with the lowest susceptibility zones (shown by black arrows) that reach very close to the surface. A good example coincides with a mapped shear zone in the middle part of the model. Towards the western end of section 1 Juhojuntti et al. (2014) reported an east-dipping structure in the seismic data at CDP 500, which may be associated with Hauki quartzite, which forms the eastern contact of the east-dipping high-susceptibility structure. This dip is not observed in the resistivity model, but corresponds with a low-density zone in the density model. It should be noted that dips from the high-magnetic structures (white) shown on the density model are reasonably collocated with the high-density zones. The resistivity and density contrast models seem to have a better depth penetration and resolve structures at depths  $>2.5$  km that are not resolved in the susceptibility model. The west-dipping low resistivity and low/intermediate density at the western end of the section (west of 740000E) and the low-density and high-resistivity features (Figs. 3B and 3C) to the east of this structure (east of 720000E) are two examples. The high-resistivity structure at depths below 3000 m, east of 720000E may be caused by intrusive rocks which, due to the density contrasts, are probably felsic intrusions.

Table 1: Summary of the estimated physical properties of various geological units and structures along section 1.

Structure/unit	Magnetic susceptibility (SI $\times 10^{-5}$ )	Resistivity (Ohmm)	Density contrast (kg/m <sup>3</sup> )
Sedimentary rocks	Low (<100)	Low (< 1000)	Low/intermediate (-0.07–0.00)
Felsic volcanic rocks	Low	Intermediate (1000–4000)	Low (<-0.07)
Mafic volcanic rocks	High (>5000)	Not resolved	High (>0.06)
Shear zones	Low	Low	Low
Granitoids	Low–intermediate	High (> 4000)	Low
Mafic intrusions	High	Very high (> 10000)	High (>0.06)

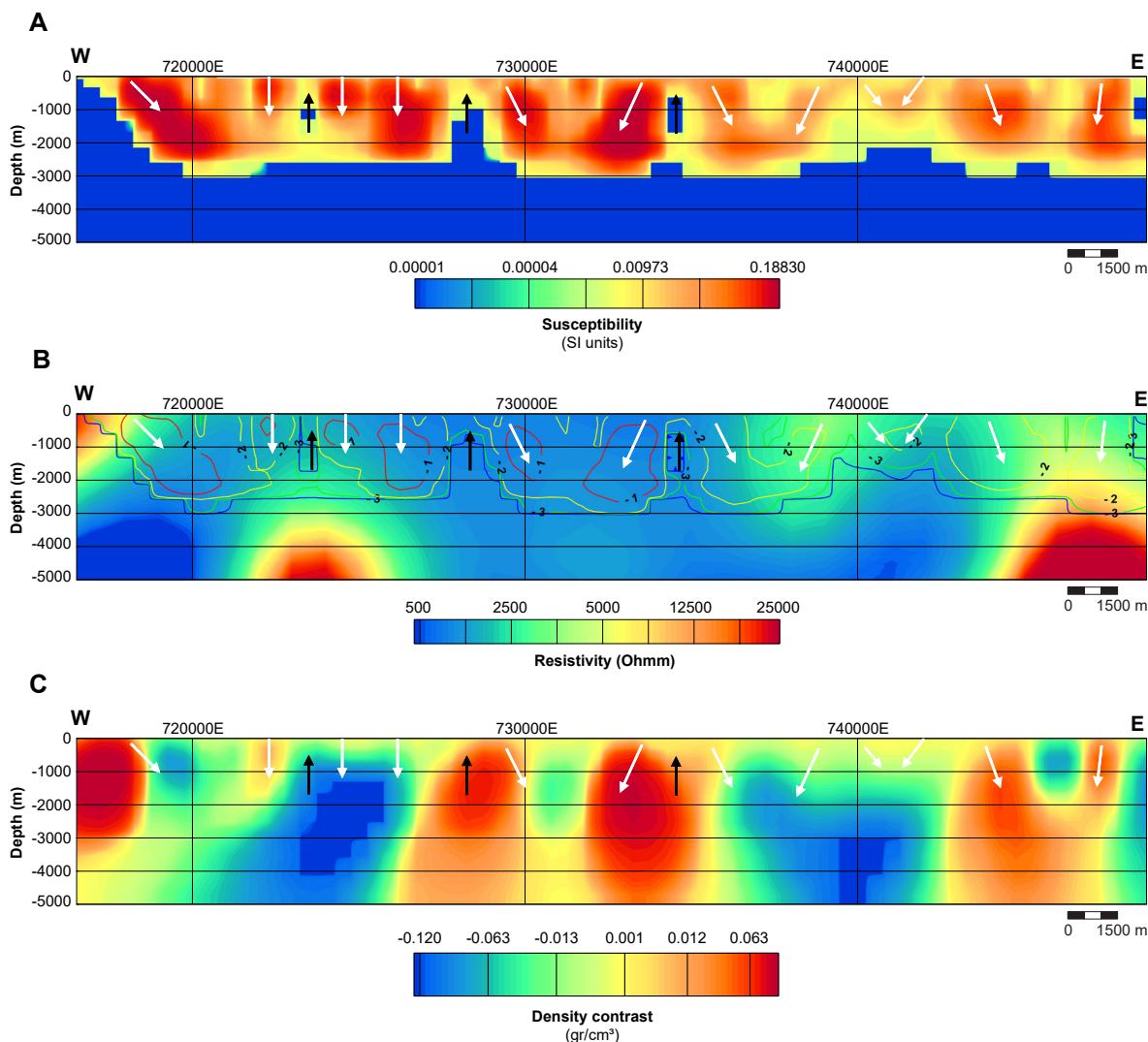


Figure 3. Sections from 3D models along section 1 shown in Figures 1 and 2. **A.** Susceptibility. **B.** Resistivity. **C.** Density contrast. In B the resistivity model is in the background and the contours with different colours represent the estimated magnetic susceptibility in logarithmic scale. The mapped bedrock and known mineralisations along each direction are shown on top of the resistivity section. The white and black arrows indicate the interpreted dips of high- and low-susceptibility zones, respectively.

### Section 2 and 3

Figure 4 shows the models along sections 2 and 3. The MT data along the nearly 15 km long section 2 has a better coverage than section 1. Table 2 shows the modelled physical properties of geological units and structures along sections 2 and 3.

Along section 2 (Figs. 3A–C) extremely high-resistivity ( $> 20\,000$  Ohm) and relatively high-susceptibility and high-density zones are resolved (west of 756000E). The high-resistivity zone continues down to a depth of approximately 4 km with a northwest-dipping trend. The same dip is observed in the susceptibility and density model. However, the magnetic model estimates a maximum depth of 3 km, and the density model a depth of approximately 3.5 km. On the geological map the first 4 km of the section in the west is marked as a gabbro intrusion with some inclusion of a granitoid. At the point of granitoid inclusion modelled resistivity decreases towards the west, and susceptibility shows some slight changes. The density model indicates low values in this interval that do not match the geological information and indicate intrusions of a more felsic nature. Towards the east of the Karesuando–Arjeplog

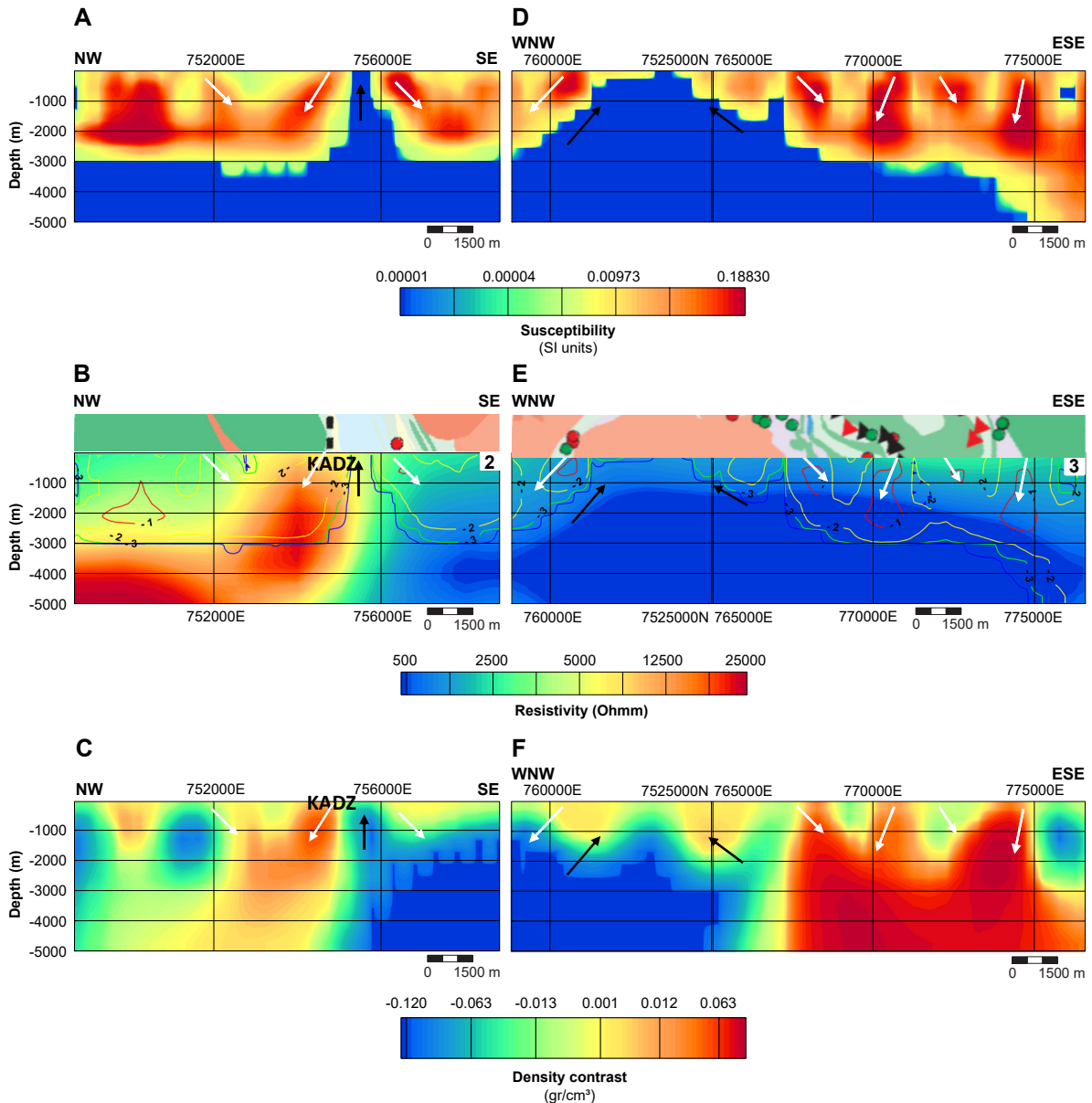


Figure 4. Sections from 3D models along portion 2 and 3 shown in Figure 1 and 2. **A.** Susceptibility. **B.** Resistivity. **C.** Density contrast along direction 2. **D.** Susceptibility. **E.** Resistivity. **F.** Density contrast along direction 3. In B and E the resistivity model is in the background and the contours with different colours represent the estimated magnetic susceptibility in logarithmic scale. The mapped bedrock and known mineralisations along each direction are shown on top of the resistivity section. The white and black arrows indicate the interpreted dips of high and low-susceptibility zones, respectively.

deformation zone (KADZ) the resistivity and density models show a dramatic change, with decreasing values, especially at deeper levels (resistivities < 500 Ohmm and density contrasts < -0.12 kg/m<sup>3</sup>). Close to this contact a few sulphide mineralisations are reported in the SGU mineral resource database. A folded structure can be seen on the magnetic anomaly map (Fig. 1B) and modelled susceptibility also suggests a folded structure in the form of a syncline that continues to a depth of approximately 2 km. It is obvious that the folded structure within the KADZ is more like an anticline fold, with a northwest-dipping, high-susceptibility structure most likely caused by highly magnetic volcanic rocks.

Section 3 is 19 km long and has a W-NW-E-SE orientation. A high-susceptibility structure dipping northwest shows up at the W-NW end of the section. Further east, the profile crosses granitic rocks

Table 2. Summary of the estimated physical properties of various geological units and structures along sections 2 and 3

Structure/unit	Magnetic susceptibility ( $\times 10^{-5}$ )	Resistivity (Ohmm)	Density contrast ( $\text{kg/m}^3$ )
Sedimentary rocks	Low (<100)	Low (< 1000)	Intermediate (0.00–0.02)
Felsic volcanic rocks	Low	Not resolved	Low (<0.07)
Mafic volcanic rocks	High (>5000)	Intermediate (1000–4000)	High (>0.06)
Karesuando–Arjeplog deformation zone (KADZ)	Low	Low	Low
Granitoids	Low–intermediate	Intermediate (1000–4000)	Low-intermediate (-0.07–0.01)
Mafic intrusions	High	Intermediate–high	High (>0.06)

with low-susceptibility contrasts. Occurrence of low-density, quartz monzodioritic rocks at the eastern gradient of the gravity low was mapped by Lynch & Jönberger (2013). Our data suggest that the intrusives here are predominantly rocks of mainly felsic composition at depth, which is confirmed by the forward modelling presented by Juhojuntti et al. (2014). At coordinates SWEREF99 TM 767971/7523890 the profile cuts the Nunasvaara area with known graphite, iron and sulphide mineralisations, the host rock being the Vittangi greenstone group. The group is dominated by volcanic, volcanoclastic and sedimentary rocks, and cut by doleritic sills. (Lynch & Jönberger 2013). The susceptibility model suggests steeply dipping, folded structures that deepen to the southeast. There is good correlation with the 2D interpretation of the gravity and magnetic data made by Juhojuntti et al. 2013. The resolution of the 3D models is 500 metres, but there are high-frequency changes in the lithology data to consider for more detailed interpretation of this specific area. The resistivity section is mainly dominated by a very low-resistivity feature east of KADZ. Resistivity decreases considerably with depth, reaching values < 500 Ohmm. Based on various reports (e.g. Lynch & Jönberger 2013, Martinsson 2011 and references therein), this area is dominated by graphite and sulphide mineralisations and, in the most easterly part, is best known for schist-hosted graphite deposits (e.g. Nunasvaara), which represent the largest known graphite resource in Sweden. The susceptibility model also indicates the presence of an extremely low-susceptibility zone at a depth > 2 km. The density section depicts a huge contrast in the middle part in which a very high-density zone that continues to depths > 5 km is resolved in the eastern part of the section. Shallower density variations indicate folded structures with dips that correlate well with those predicted by the susceptibility model. High densities and high susceptibilities may be directly related to the mafic volcanics and intrusions mapped in the area. The very low-density zone at depth in the western part of the density model may be caused by a granitic intrusion observed in the area. Two scenarios are suggested for the deep and very low-resistivity feature that starts at 756000E and continues to the end of section 3: a) the highly conductive mineralisations observed in the area (Martinsson 1993); or b) a deep-seated rock type with low resistivity, susceptibility and density. The latter is considered more likely due to the geometry and extent, although the extremely low resistivity is hard to explain. This is a scientific question to be answered by future research.

#### Section 4

This is the longest section (38 km) and crosses a variety of geological units and structures (Figure 5 A–C). Table 3 summarises the physical properties of various rock types and structures along section 4.

Although the low-susceptibility feature/zone at depth (> 2 km) correlates well with another low-resistivity zone in the northwestern part of the section, the density model suggests that this zone has a very high-density material at depth. The sole explanation for this may be the presence of highly conductive, low-susceptibility and high-density sulphide mineralisations.

In the density model the low-density felsic volcanic rocks (e.g. at 7540000N) affect the model due

Table 3. Summary of the estimated physical properties of various geological units and structures along section 4

Structure/unit	Magnetic susceptibility ( $SI \times 10^{-3}$ )	Resistivity (Ohmm)	Density contrast ( $kg/m^3$ )
Sedimentary rocks	Low (<100)	Low (< 1000)	Intermediate (0.00–0.02)
Felsic volcanic rocks	Low	Not resolved	Low (<-0.07)
Mafic volcanic rocks	High (>5000)	Intermediate (1000–4000)	High (>0.06)
Karesuando–Arjeplog deformation zone (KADZ)	Low	Low	Low
Granitoids	Low–intermediate	Intermediate (1000–4000)	Low–intermediate (-0.07–0.01)
Mafic intrusions	High	Intermediate–high	Intermediate to high (0.03–0.06)

to coarser data sampling than in the susceptibility model. This affects the comparison between the apparent estimated dips for the high-susceptibility structures that are superimposed on the density model along this section. There are a few cases where the high-susceptibility dips are collocated with low-density zones in the density model. The rhyolitic low-density rocks at SWEREF99 TM 739527/7531904 appear to dip below the mafic basaltic rocks to the northwest, which could explain the low-density contrast.

High-density basalts and andesites of considerable depth appear in the northwest of the profile. It is not clear what rocks are responsible for the density low within the high-density area at SWEREF99 TM 725475/7544910, due to the lack of outcrop, but they are probably the quartz-rich sedimentary rocks to the southwest continuing to the northeast. In the susceptibility models, and to some extent in the density contrast model, mafic volcanic rocks appear folded and have deeper roots than the felsic volcanic rocks. Volcanic rock sequences of felsic and mafic composition follow with low and high-density areas, respectively. At coordinates SWEREF99 TM 732994/7537950 high-density and high-susceptibility structures occur but cannot be correlated with the trachyte-rhyolites on the geological map.

To the southeast, close to 740000E, all three models demonstrate a sharp contrast/change. In the susceptibility model, two distinct, rather high-susceptibility zones that continue down to depths > 3 km coincide with a resistivity zone with intermediate to high-resistivity dipping towards the north-northwest (Fig. 5B). Both zones become shallower in the most easterly parts of the sections. The density model (Fig. 5C) correlates well with the information shown on the geological map. A low-density zone is sandwiched between two higher-density zones that can be correlated to the granitic and gabbroic intrusions, respectively. The low-density zone appears to have deeper roots than the denser zones, implying that the granites might continue deeper than their gabbroic counterparts. This low-density zone relating to the granitic intrusion correlates well with the low-susceptibility zone resolved by the magnetic model (Fig. 5A).

## Section 5

This section has an almost north–south orientation, is 31 km long and crosses two shear zones, as well as various felsic and mafic intrusions and volcanic rocks. A summary of the physical properties of the geological features mentioned above is given in Table 4.

In the northern part of the sections a clear low-susceptibility, intermediate resistivity (1000–4000 Ohmm) and very low-density (density contrast <-0.12) structure/feature that continues down to depths > 5 km is prominent (Fig. 6A–C). It dips approximately 45 degrees to the SE. At the location marked by a shear zone on the geological map, a sharp boundary can be observed in almost all sections. Towards the south of the shear zone a high-susceptibility and density zone is apparent, and appears deeper in the density model. The zone is not resolved in the resistivity model because of very poor data coverage in this area (see Fig. 1). Further to the south, a zone marked by two vertical and one horizon-

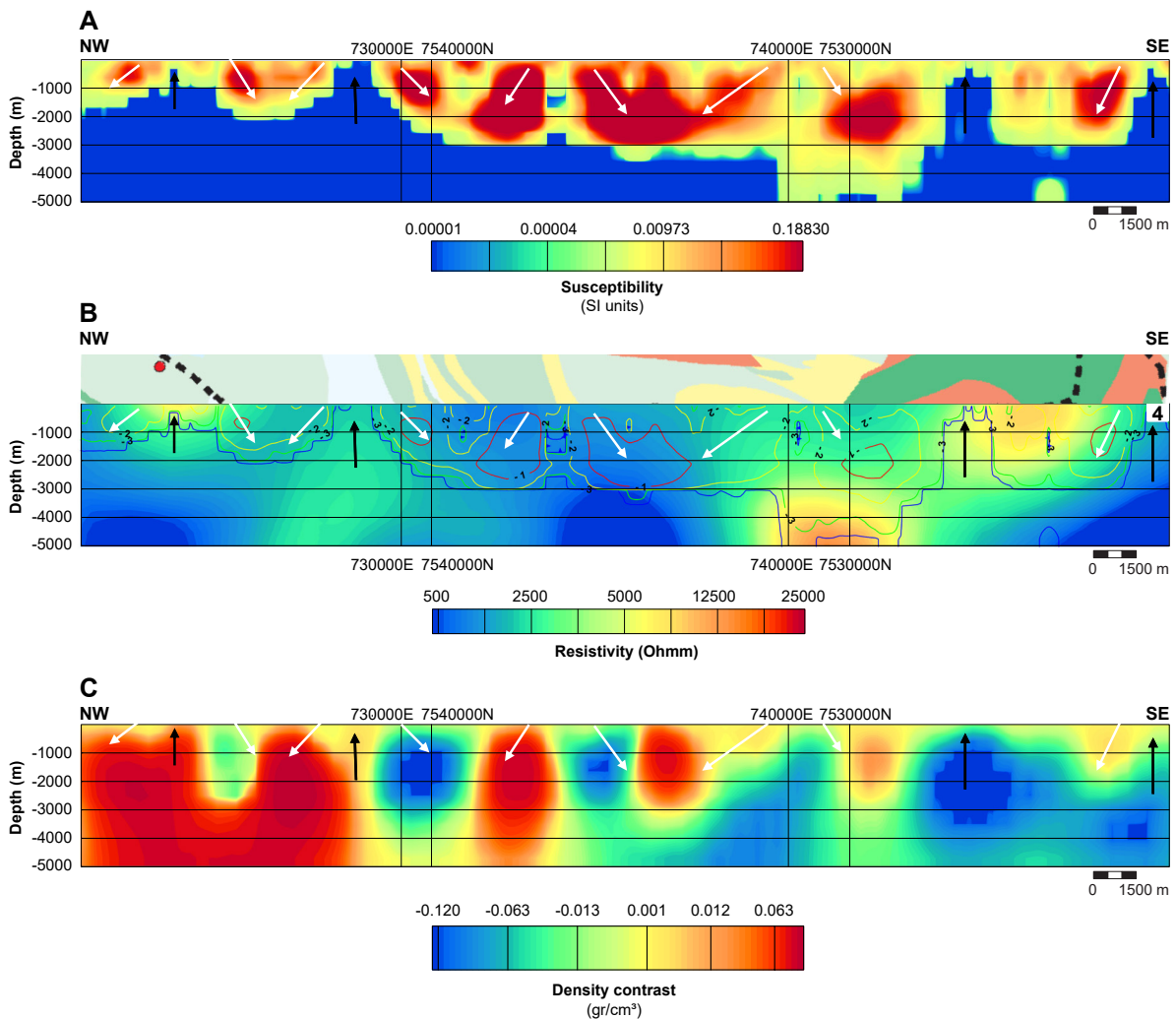


Figure 5. Sections from 3D models along portion 4 shown in Figures 1 & 2. **A.** Susceptibility. **B.** Resistivity. **C.** Density contrast. In B the resistivity model is in the background and the contours with different colours represent the estimated magnetic susceptibility in logarithmic scale. The mapped bedrock and known mineralisations along each direction are shown on top of the resistivity section. The white and black arrows indicate the interpreted dips of high and low-susceptibility zones, respectively.

Table 4: Summary of the estimated physical properties of various geological units and structures along section 5

Structure/unit	Magnetic susceptibility ( $\times 10^{-3}$ )	Resistivity (Ohmm)	Density contrast ( $\text{kg/m}^3$ )
Sedimentary rocks	Low (<100)	Intermediate–high	Intermediate (0.00–0.02)
Felsic volcanic rocks	Low or not resolved	Not resolved	Low or not resolved
Mafic volcanic rocks	High (>5000)	High (>10000)	High (>0.06)
Karesuando–Arjeplog deformation zone (KADZ)	Low	Not resolved	Low (< -0.07)
Granitoids	Low	Intermediate (1000–4000)	Low to very low
Mafic intrusions	High	Low to high	Intermediate to high (0.03–0.06)

tal arrow (Figs. 6A–C) is noted. At the top a 200–300 m thick, moderately dense and magnetic layer is apparent. Below this, a very low-susceptibility (almost zero), high-resistivity (>10 000 Ohmm) and low to intermediate density structure continues to depths >5 km. A syncline-shaped high-susceptibility and moderately high-density structure is resolved north of KADZ. This may be associated with the mafic volcanic rocks mapped in this part of the section. The northern limb dips more gently and the folding is more pronounced in the magnetic model, probably due to better data coverage. It should be borne in mind that the section crosses the magnetic anomalies at a high angle, which may generate

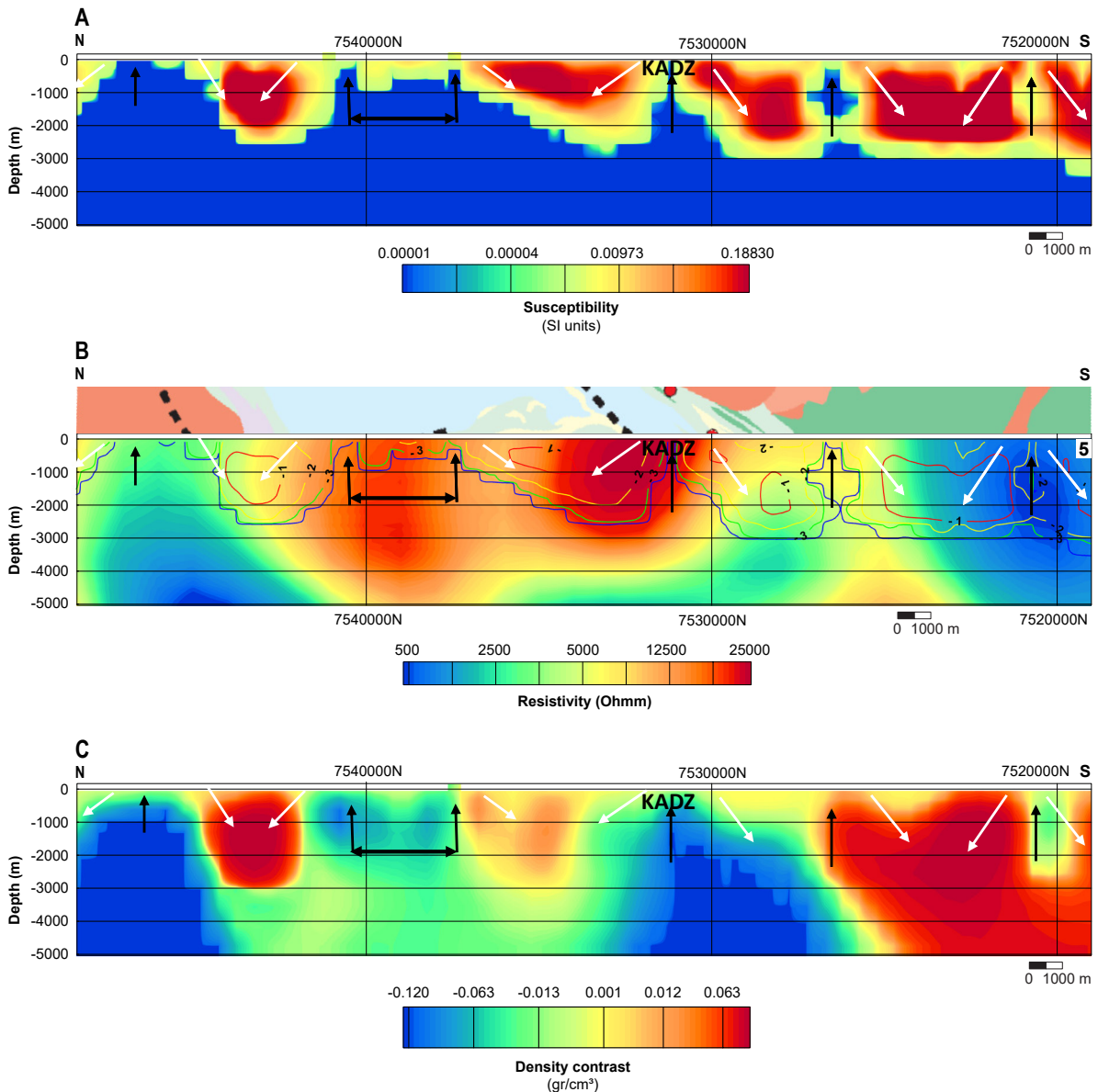


Figure 6. Sections from 3D models along section 5 shown in Figures 1 & 2. **A.** Susceptibility. **B.** Resistivity. **C.** Density contrast. In B the resistivity model is in the background and the contours with different colours represent the estimated magnetic susceptibility in logarithmic scale. The mapped bedrock and known mineralisations along each direction are shown on top of the resistivity section. The white and black arrows indicate the interpreted dips of high and low-susceptibility zones, respectively.

“false” synforms, showing instead the plunging hinge of a fold in the southeastern part of the anomaly.

As in sections 2 and 3, the KADZ is also pronounced in the susceptibility and density sections, showing sharp changes with extremely low values. However, it is not so pronounced in the resistivity model at that exact location of the KADZ, but a few kilometres towards the north a NW-dipping low to intermediate zone is seen. The susceptibility and density highs at the southern end of the section (SWEREF99 TM 748233/7525845) coincide with a mafic gabbro-diorite intrusion. Contact between the gabbro and the granites dipping to the northwest is seen in both sections. Surprisingly, a very low-resistivity zone is modelled in the last 3 km of the southern end of the section at the contact between the granite and gabbro. On the magnetic field anomaly map a highly negative lineament occurs in this zone.

## Comparison with reflection seismic sections

We compare the models shown along sections 1, 2, and 3 with the migrated reflection seismic sections reported by Juhojuntti et al. (2014). Along sections 1 and 3 we compare the susceptibility and density contrast models, whereas along section 2 the resistivity model is also included. The comparison is mainly qualitative because much more detail is seen in the seismic sections due to the higher data sampling density. We show the seismic section on top of the selected models and use arrows and broken lines to indicate the most dominant reflection patterns, i.e. the stronger reflections that are clearer in the seismic sections. Figure 7 shows seismic section 1. The broken black line marks the bottom of shallower reflections above a depth of approximately 1 km, where the reflectivity is substantially higher. The smaller arrows show the apparent dip of dominant reflections. In the depth range 0–1 km, the apparent dip of shallower reflections mostly accords reasonably well with those seen in the susceptibility and density contrast models. However, dips are gentler in the seismic section (compare with those shown in Figs. 3A and 3C). Below 2 km, the susceptibility model does not resolve any contrast and the best comparison is made between the density contrast model and the reflection seismic sections. Generally speaking, below this depth the reflections are weaker and sparser. In the west, an almost horizontal high-reflectivity zone predominates at > 4 km, while to the east, after 720000E, a 45-degree west-dipping high-reflectivity zone clearly predominates until 730000E. This higher-reflectivity zone coincides very well with the low and high-density zones with approximately the same dips. Further east, the dominant dip of the high-reflectivity zone changes towards the east, coinciding with a high-density zone (Fig. 7B). We have marked with “?” two deeper reflectivity zones that seem to be artefacts dictated by the migration process. The east-dipping reflection trend predominates to the eastern end of the section and no significant correlation can be seen with either the susceptibility or the density contrast models.

Figure 8A–C shows the comparison between susceptibility, resistivity, density contrast models and the reflection seismic data along section 2. The apparent dips of shallower reflections (marked by smaller arrows) correlate well with the highs and lows seen in the susceptibility model (Fig. 8A) and to some extent with the structures seen in the density contrast model (Fig. 8C). In the depth range 1–3 km, the first third of the section in the NW, a moderately SE-dipping high-reflectivity trend (marked by a long arrow) predominates in the seismic section and coincides best with the high-susceptibility zone. Further SE the dip changes to the NW, which can be interpreted as a regional syn-

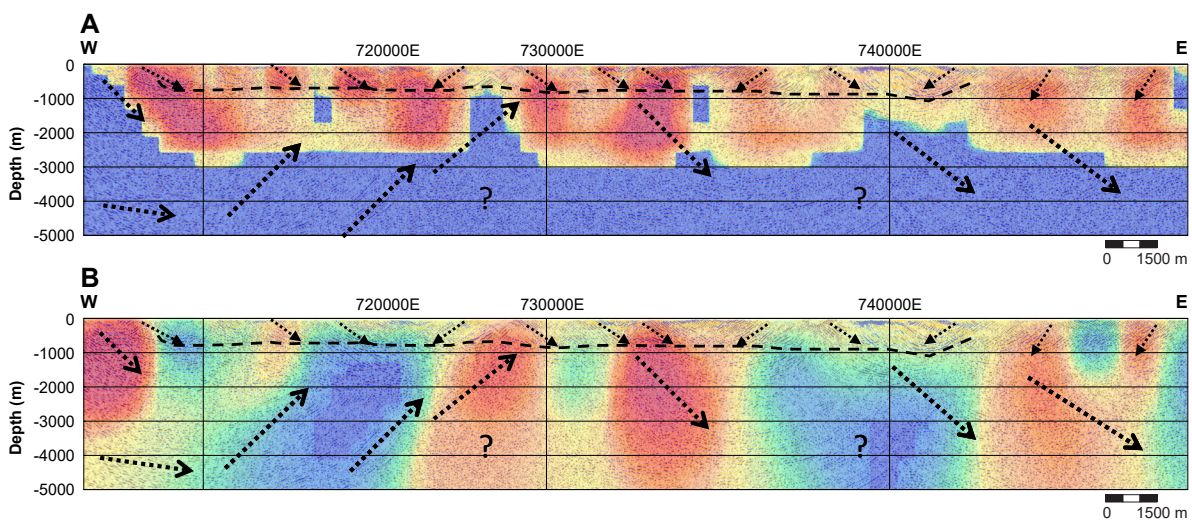


Figure 7. Comparison between the migrated seismic section with **A** the susceptibility model and **B** the density contrast model along section 1. The smaller arrows indicate shallower and more local predominant trends. The longer arrows represent deeper reflections. The broken black line marks the bottom of a shallower high-reflectivity zone in the seismic section. The “?” shows possible artefacts caused by migration.

clinal structure. NW-dipping strong positive susceptibility, positive density contrast and a high-resistivity zone are clearly observed in this part of the sections (Figs. 8A–C). With the exception of a few shallow diffractions in the seismic section, the KADZ is not resolved as clearly as in the other sections. Towards the SE of the KADZ the regional dip trend in the seismic section reverts towards the SE. It should be noted that at the deeper levels in this part of the section (> 3 km) fringe-shape reflection may have been introduced by the migration processes.

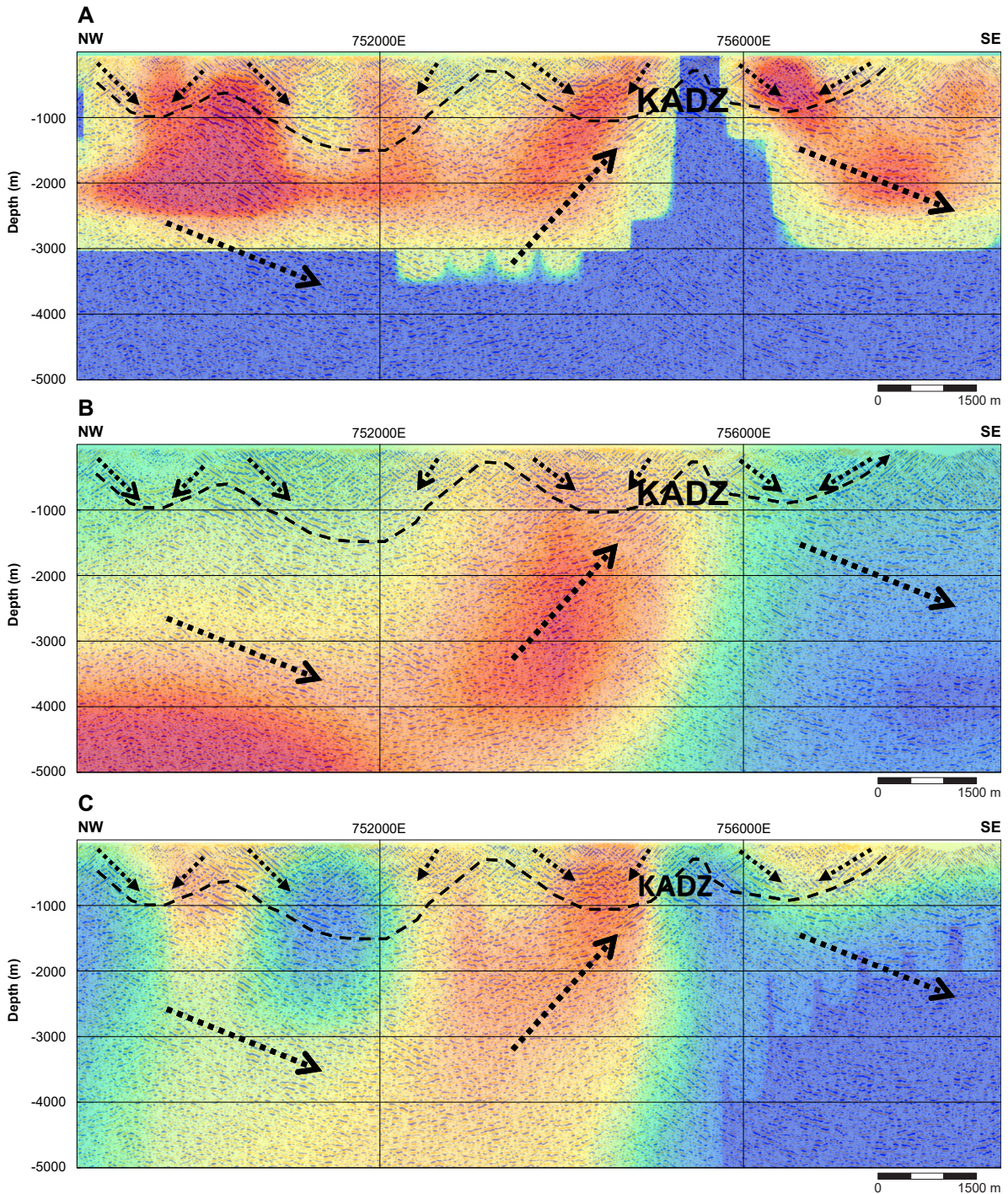


Figure 8. Comparison between the migrated seismic section with **A** susceptibility model, **B** resistivity model and **C** density contrast model along section 2. The smaller arrows indicate shallower and more local predominant trends. The longer arrows represent deeper reflections. The broken black line marks the bottom of a shallower high-reflectivity zone in the seismic section.

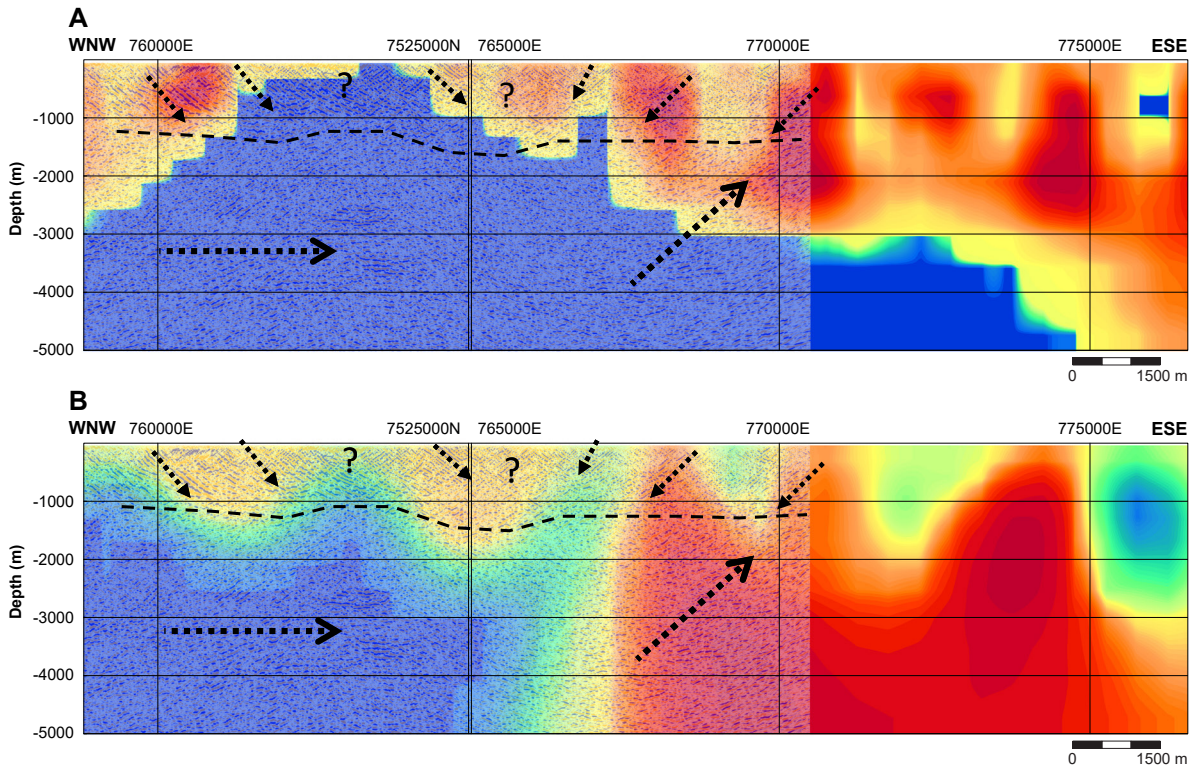


Figure 9. Comparison between the migrated seismic section with **A** susceptibility model and **B** density contrast model along section 3. The smaller arrows indicate shallower and more local predominant trends. The longer arrows represent deeper reflections. The broken black line marks the bottom of a shallower high-reflectivity zone in the seismic section. The “?” shows possible artefacts caused by migration.

The seismic data cover the first two-thirds of section 3 (Fig. 9). The apparent dip of shallower reflections is dominated by E-SE and W-NW trends in the first and second half of the section, respectively. The deeper reflections show varying dips in the first half of the section, whereas the second half is dominated by a W-NW-dipping high-reflectivity zone that starts at the position where an almost vertical high-density zone appears in the density model. High-density mafic volcanic and gabbro intrusions are mapped at this boundary. Two very distinct almost horizontal reflectors, marked by a long horizontal arrow at a depth of 2.5–3.5 km, are of great importance in the seismic section. These were interpreted as smaller mafic bodies in the forward model presented by Juhojuntti et al. (2014). Neither the magnetic nor the gravity inversion model reveals such a distinct zone, although a weak gradient in the density contrast model can be distinguished in that area.

Figure 10 shows a more regional summary of the estimated apparent dips along sections 1 to 5 taken from the magnetic susceptibility models and seismic sections (1–3) shown on the geological maps in the area. The black arrows point towards the down-dip. Note that the dips are presented for moderate to high-susceptibility structures. In our interpretations we have also taken some account of the density and the resistivity models where the dips are not well resolved by both datasets. A few arrows might represent the steeply dipping structures that are shown in the magnetic models with vertical arrows. The reader is referred to the discussions made to compare the dips with those seen in the density contrast models. The thicker broken line marked by a “?” indicates possible continuation of the shear zone mapped in the NE and crossing section 5. This approach can be applied to the entire model area to construct a more detailed image of variation of the dip direction. To verify the validity of our dip interpretations we have compared them with an analysis made by Eriksson & Hallgren (1975). The folds (anticlines and synclines) interpreted by their study are shown in Figure 10 by red

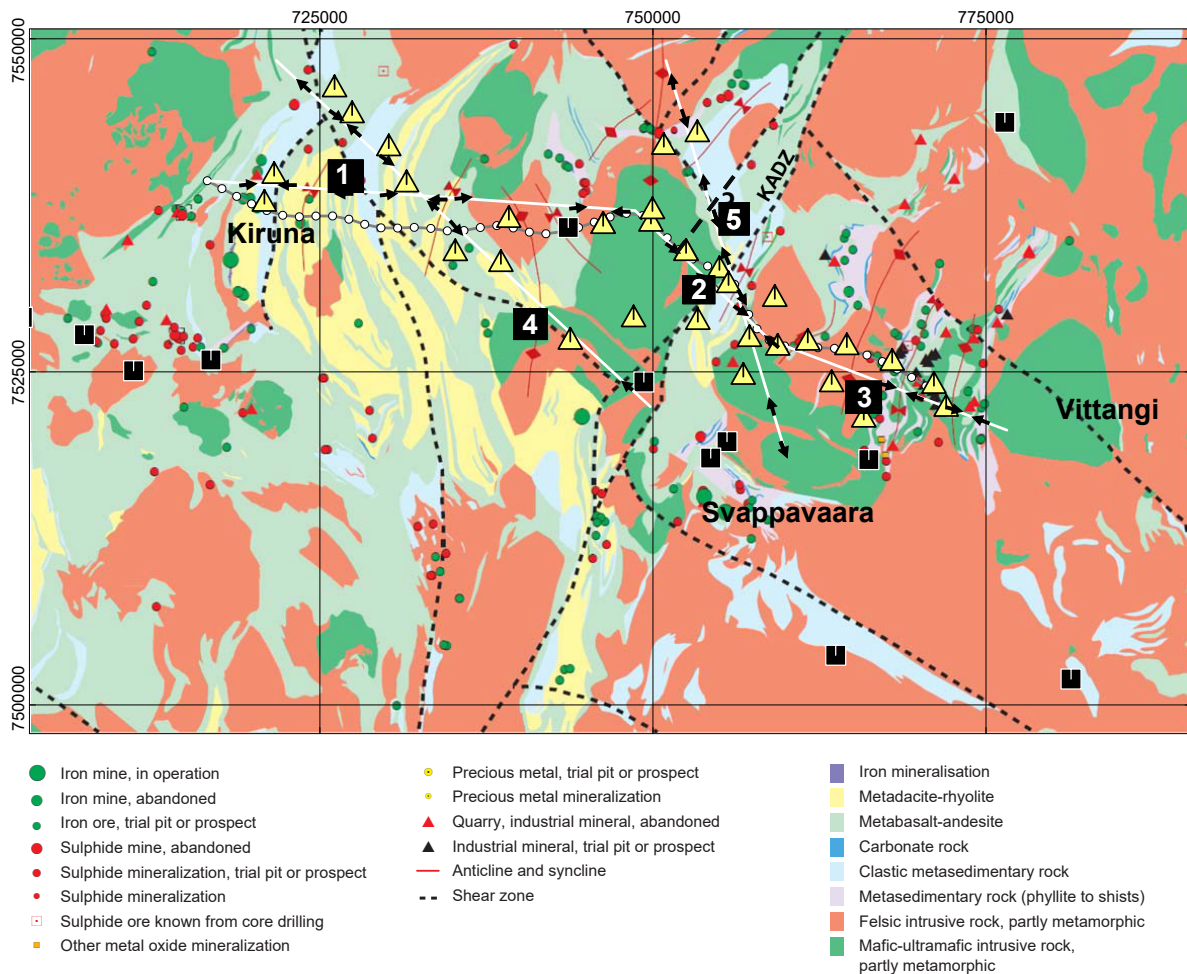


Figure 10. Regional presentation of the estimated dips of structures with moderate to high magnetic susceptibilities taken from the 3D inversion results. Most of the dips are confirmed by the reflection seismic data.

symbols. We generally find a good correlation between the geological structures presented by Eriksson & Hallgren (1975) and those derived by interpreting models from different geophysical responses. However, there are also some differences, giving us new information and insights. In the middle part of section 1, east of 730000E, the susceptibility model suggests an anticline (Fig. 3A). The same pattern (Fig. 5A) is also observed in section 4, near the intersection with section 1, while the geological observations reported by Eriksson & Hallgren (1975) show a synclinal structure (Fig. 10). This is also the case along the eastern part of KADZ (Fig. 10) where sections 2 and 5 cross each other. The susceptibility and the density sections show an anticline (Fig. 4A, C and Fig. 6A), c), whereas the geological model/interpretation shows a syncline (Fig. 10). In this case, the seismic section also suggests an anticline structure at depth (Fig. 8). It should be noted that the geological observations and geophysical models have somewhat different scales, which gives rise to different interpretations.

## CONCLUSION

The models from 3D inversions of the potential field and the MT data demonstrate a reasonable correlation with geological units and mineralised zones in the area. As expected, shear zones appear as low-resistivity, low-susceptibility and low-density zones in the selected sections from the 3D models. High-susceptibility and high-density zones mark the basaltic volcanics and in most of the cases, appear as high-resistivity zones in the resistivity models. A very distinct low-resistivity and low-susceptibility zone of varying density (high and low) is observed in the eastern part of section 3, where zones of sulphide and graphite mineralisations are known. The MT method has a poor resolution at shallower depths but a reasonably deep depth penetration. The 3D resistivity models can be used to study geometry and properties of deep-seated crustal structures as deep as 50 km. The susceptibility models, on the other hand, demonstrate a very high-resolution near the surface and are best for comparison with the high-resolution reflection seismic data for the study of shallower structures and geological units. Dips estimated using the susceptibility models accord fairly well with those from seismic data. However, the smoothing regularization used in the 3D modelling and the coarser sampling of the magnetic data led to big differences in some portions of the sections. The density, resistivity and reflection seismic data correlate best in deeper parts of the models. This suggests they may be preferred when constructing a 3D model for more regional structures residing at depths >2 km. The dips interpreted from integrated use of geophysical models correlate reasonably well with previous geological interpretations made from field observations. But there are differences that might be due to the difference between the scales used in the modelling. These differences give us new information and insights thanks to the ability of geophysical models to resolve deeper information.

## OUTLOOK

This study suggests that models from independent 3D inversions of the geophysical data contain valuable information that can be used for imaging and classifying geological structures in 3D. The methods used here have different sensitivities and, when inverted jointly, can produce models with even more reliable information. Joint inversion of MT and gravity data has become a common practice and can be tried on these datasets. The valuable detailed structural information found in the reflection seismic data can be applied in the inversion of magnetic field data as constraints or *a priori* information to estimate the geometry of the geological structures more accurately. We suggest a detailed electromagnetic survey with higher frequencies, such as a controlled source and radio magnetotelluric survey, to collect supplementary information to better understand the depth and lateral extent of the low-resistivity mineralised zones close to Vittangi village. The cause of a deep and extremely low-resistivity, low-density and low-susceptibility zone in the middle of section 3 is unknown and should be the subject of more scientific research.

## ACKNOWLEDGEMENTS

Dr. Maxim Smirnov of Olou University (currently at Luleå University of Technology) kindly provided us with existing MT stations close to the study area.

## REFERENCES

- Arora, K., Tiwari, V.M., Singh, B., Mishra, D.C. & Grevemeyer, I., 2012: Three dimensional lithospheric structure of the western continental margin of India constrained from gravity modelling: implication for tectonic evolution, *Geophysical Journal International* 190, 131–150, doi:10.1111/j.1365-246X.2012.05506.x
- Aster, R. C., Borchers, B. & Thurber, C.H., 2005: *Parameter estimation and inverse problems*: Academic Press.
- Bastani, M., Antal Lundin, I., Savvaidis, A., Kamm, J., & Wang, S., 2015: Audiomagnetotelluriska (AMT) mätningar i Kiruna- och Lannavaaraområdet, preliminära resultat. *Sveriges geologiska undersökning SGU-rapport 2015:10*, 16 p.
- Bergman, S., Kübler, L. & Martinsson, O., 2000: Regional geological and geophysical maps of northern Norrbotten County: Bedrock map (east of the Caledonian orogen). *Sveriges geologiska undersökning, Ba 56:1*.
- Bergman, S., Kübler, L. & Martinsson, O., 2001: Description of regional geological and geophysical maps of northern Norrbotten County (east of the Caledonian orogen). *Sveriges geologiska undersökning Ba 56*, 110 pp.
- Cherevatova, M., Smirnov, M.Yu., Jones, A.G., Pedersen, L.B. & MaSca Working Group, 2015: Magnetotelluric array data analysis from north-west Fennoscandia, *Tectonophysics* 653, 1-19, doi:10.1016/j.tecto.2014.12.023
- England, R. W. & Ebbing, J. 2012: Crustal structure of central Norway and Sweden from integrated modelling of teleseismic receiver functions and the gravity anomaly. *Geophysical Journal International* 191 (1): 1–11. doi:10.1111/j.1365-246X.2012.05607.x
- Eriksson, B. & Hallgren, U., 1975: Berggrundsgelogiska och flygmagnetiska kartbladen Vittangi NV, NO, SV, SO. *Sveriges geologiska undersökning Af Nr 13–16*.
- Hedin, P., Malehmir, A., Gee, D., Juhlin, C. & Dyrelius, D., 2014: 3D interpretation by integrating seismic and potential field data in the vicinity of the proposed COSC-1 drill site, central Swedish Caledonides. *Geological Society Special Report, Geological Society*. 390, 301–319.
- Juhonjuntti, N., Olsson, S., Bergman, S. & Antal Lundin, I., 2014: Reflexionsseismiska mätningar vid Kiruna – preliminär tolkning. *Sveriges geologiska undersökning SGU-rapport 2014:05*, 26 p.
- Kamm, J., Antal Lundin, I., Bastani, M., Sadeghi, M. & Pedersen, L., 2015: Joint inversion of gravity, magnetic and petrophysical data – A case study from a gabbro intrusion in Boden, Sweden. *Geophysics*, 80(5): B131–B152.
- Lynch, E. P., & Jönberger, J., 2013: Summary report on the geological and geophysical characteristics of the Nunasvaara key area (29K Vittangi NO & SO). *Sveriges geologiska undersökning, SGU-rapport 2013:11*, 35 p.
- Martinsson, O., 1993: Greenstone and porphyry hosted ore deposits in northern Norrbotten. *PIM/NUTEK report # 1*, 77 p.
- Martinsson, O., 1997: Paleoproterozoic greenstones at Kiruna in northern Sweden: a product of continental rifting and associated mafic-ultramafic volcanism. In: O. Martinsson: *Tectonic setting and metallogeny of the Kiruna greenstones. Doctoral thesis 1997:19, Paper I*, 1–49. Luleå University of Technology.
- Martinsson, O., 1999: Berggrundskartan 30J Rensjön SO, skala 1:50 000. *Sveriges geologiska undersökning Ai 133*.
- Martinsson, O., 2011: Kiskamavaara: a shear zone hosted IOCG-style of Cu-Co-Au deposit in Northern Norrbotten, Sweden: 11<sup>th</sup> Biennial SGA meeting, Antofagasta, Chile.
- Öhlander, B., Skiöld, T., Elming, S.-Å., BABEL Working Group, Claesson, S. & Nisca, D.H., 1993: Delineation and character of the Archaean-Proterozoic boundary in northern Sweden. *Precambrian Research* 64, 67–84.
- Siripunvaraporn, W., Egbert, G., Lenbury, Y. & Uyeshima, M., 2005: Three dimensional magnetotelluric inversion: Data-space method. *Physics of the Earth and Planetary Interiors* 150, 3–14, doi: 10.1016/j.pepi.2004.08.023.



Geological Survey of Sweden  
Box 670  
SE-751 28 Uppsala  
Phone: +46 18 17 90 00  
Fax: +46 18 17 92 10  
[www.sgu.se](http://www.sgu.se)

Uppsala 2018  
ISSN 0349-2176  
ISBN 978-91-7403-393-9  
Tryck: Elanders Sverige AB